AIAA JOURNAL
Vol. 57, No. 4, April 2019

Topology Optimization of Solid Rocket Fuel

Trenton Kirchdoerfer* and Michael Ortiz†
California Institute of Technology, Pasadena, California 91125
and
Donald S. Stewart‡
University of Illinois, Urbana, Illinois 61801

DOI: 10.2514/1.J057807

This paper investigates possible improvements in the combustion properties of multicomponent solid propellants through the application of topology optimization methods to representative volume element (RVE) of HMX-aluminum fuel. Design objectives for the material include increased thermal conductivity and reduced amounts of induced strains under thermal loads. The targeted increases in thermal conductivity generate designs that increase burn propagation rates, whereas the reductions in structural compliance minimize relative displacements within the design cell. Novel domain-filter treatments are also developed to better control the boundary effects on the resulting designs. A family of wire-like solutions is found to provide optimal combustion and structural properties. Burn performance estimates showed 52 and 33% improvements in burn propagation speeds relative to previous designs at, respectively, 20 and 200 atm.

Nomenclature

$\boldsymbol{C}$	=	conductivity matrix
c_p	=	heat capacity, kJ/(kg · K)
E	=	Young's modulus, GPa
$\boldsymbol{F}$	=	external forces
f	=	total design objective
f_c	=	thermal conductivity objective
f_s	=	structural objective
$\boldsymbol{H}$	=	external heat fluxes
H_{ei}	=	un-normalized filter weights
K	=	thermal conductivity, W/(m·K)
$\boldsymbol{K}$	=	stiffness matrix
MW	=	molecular weight
R	=	thermal resistivity
r_{ei}	=	radius from element e to element i
$r_{\max}$	=	filter radius of cutoff
$\boldsymbol{T}$	=	temperature, °C
T_f	=	final temperature (post combustion), K
$\boldsymbol{U}$	=	displacement, μm
V	=	volume of material
V_0	=	total volume
$V^f_{\min}$	=	minimum volume fraction
$V^f_{\max}$	=	maximum volume fraction
V^f_{HMX}	=	volume fraction of HMX
V^f_{Al}	=	volume fraction of Aluminum
w_N	=	width of null boundary domain
w_s	=	structural objective weight
$\boldsymbol{x}$	=	design variable
x_B	=	boundary of mesh
x_i	=	components of $\boldsymbol{x}$
x_r	=	location of reflective boundary
$\tilde{\boldsymbol{x}}$	=	filtered design variable
$\tilde{x}_e$	=	components of $\tilde{\boldsymbol{x}}$
α	=	thermal expansion coefficient, K^{-1}
ν	=	Poisson ratio
ρ	=	density, kg/m^3

Received 9 August 2018; revision received 5 November 2018; accepted for publication 6 November 2018; published online 29 January 2019.

*1200 E. California Blvd., MC 105-50; tkirchdo@caltech.edu.
†1200 E. California Blvd., MC 105-50.
‡268 Mechanical Engineering Bldg.

I. Introduction

SOLID rocket propellants have long offered a compelling and mechanically simple solution for providing high-thrust rockets. To date, the attempts to create more efficient solid rocket propellants have relied heavily on extensive trial-and-error tests over broad classes of chemical constituents. After the introduction of Asphalt-based propellants in 1942, solid propellants saw significant and steady improvements in specific impulse through the introduction of high-energy fuels in the 1980s [1], after which such improvements have been limited. Present research in solid propellants primarily focuses on better understanding fundamental combustion processes with aim of eventually suggesting more chemically optimal rocket constituents. However, even well-identified chemical processes retain alternative opportunities for improvements in fuel performance. The focus of this work is to demonstrate the design of a multicomponent rocket fuel through the shape optimization of a repeatable cell geometry, as sketched in Fig. 1. Modern manufacturing techniques have allowed for the design and construction of geometries with extremely small features [2,3], thus leading this work to make a general query about how to best optimize solid propellants in a more flexible design environment. And while the importance of the metal particle size, as it relates to specific impulse, has been understood since the 1960s [4], particle geometries exist as an extreme subset of the potential geometric design space.

What remains then is to identify properties of interest that might improve engine performance. In this work, we rely on the positive dependence of burn-front mass flux on thermal conductivity in monopropellants [5–7]. For example, the steady-state Merzhanov formula for a monopropellant controlled by condensed phase reactions shows that the mass flux is proportional to the square root of the thermal conductivity. In this work, we assume that by design we can affect changes in the effective properties and thus estimate performance properties using correlations and estimates based on simple combustion models for homogenized propellant. We have used the model found in [7] to roughly estimate changes in the regression rate, as seen in Sec. IV.C, as the effective properties of the propellant are changed in the design. Thus, by increasing thermal conductivity and reducing structural compliance, we directly affect and estimate improvements in the chemical and structural performance of multicomponent fuels. To realize such improvements through the selection of component geometries, we then turn to the field of topology optimization to supply specific designs.

Topology optimization methods provide designers a well-developed framework for optimizing design variables with regard to improving design objectives. Such objectives are then described by compliance functionals that, when minimized, result in optimal solutions [8]. Within our specific problem, the design variables are the material occupancies of the respective fuel components

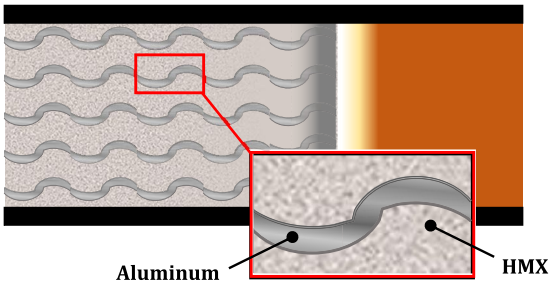

Fig. 1 Sketch of repeatable cell for combustion.

throughout the domain. Further, the volume fraction of constituents is set by a defined chemical process and represents a principle constraint on any potential solution. By then applying boundary conditions and geometry constraints to a representative volume element (RVE), we can find optimal fuel geometries.

In this paper we make use of (design) density-based, multi-objective, topology optimization routines to explore potential designs for an HMX-aluminum solid propellant. Conductivity is maximized through the minimization of a thermal compliance objective under a thermal gradient that is enforced along the burn propagation axis of the material. This is selected to best improve burn performance in direction normal to the burn interface without regard to transverse thermal conductivity. Similarly, structural compliance is minimized under a uniform thermal expansion, with a representative tank pressure applied at the free face of an otherwise symmetrically constrained RVE. Such a constraint will minimize the relative deflections of the loaded system and better maintain the design geometries as the burn front approaches a given section of material. By systematically weighting these competing objectives, families of solutions are then generated for further evaluation.

Beyond identifying properties for optimization and a desired mixing ratio, there remains a need to restrict scales of feature complexity to maintain both the method convergence and the manufacturability of the generated designs. The detail in the diagram shown in Fig. 1 shows a design of limited complexity, which is required to reduce complications that might arise when constructing the suggested solutions. Within topology optimization the use of spatial filters is used to affect such complexity restrictions for density-based methods [9,10]. Despite their common application, domain filters have not traditionally admitted the definition of filter boundary conditions. Filters without such treatments create boundary biases that violate defined scale restrictions and cause solutions to favor boundary cells. Previous work [11] has identified and removed these biases; however, using the improved methods prevented solvers from finding solutions in this work. By systematically reintroducing a controllable boundary bias, solutions can be found while limiting the boundary bias effect.

Final solutions ultimately result in two families of designs, with wire-like designs along the burn axis favoring thermal conductivity, while burn-front parallel-plate designs minimize the relative deflections. Ultimately, wire-like designs provide the most benefit burn performance, offering 52 and 33% improvements in burn propagation speeds relative to volumetrically equivalent spherical particle reference design at tank pressures of 20 and 200 atm. Such potential improvements in fuel performance suggest a promising new front in the development of advanced composite fuels.

The structure of the paper is as follows: Discussion begins with a brief review of relevant aspects of topology optimization, followed by the introduction of a controlled boundary filter bias, with further discussion included in the Appendix. Focus then moves to the specific setup of the geometry constraints, material properties, and boundary conditions used to optimize the fuel design. The design results are presented with an emphasis on the trends in the geometries and material properties that would lead to the greatest propellant improvements. Preliminary calculations follow, which then demonstrate the efficacy of improving the targeted characteristics. Conclusions focus on the possible fuel improvements derived from topology optimization design strategies and the future work suggested by these results.

II. Topology Optimization

A. Density Methods

Topology optimization methods are posed as the minimization of an objective function taken over a set of design variables, subject to design constraints and boundary conditions. For the generation of arbitrary geometries within a defined spatial domain, we take the design variables to be the material occupancy throughout the domain. Occupancy of a material is an inherently discrete property that inherently prevents the use of gradient-based solvers. Density methods represent a popular class of methods wherein this problem is simplified by treating occupancy of two material systems as a continuous variable, thus broadening the family of available numerical solution methods. Having made the concession of treating the variables as smooth, we then seek to drive their values toward designs with discernible occupancies. To do this, solver sensitivities are created by choosing interpolation schemes, driving solutions away from intermediate material occupancy values. This work uses the Solid Isotropic Material with Penalization (SIMP) [12,13] interpolation scheme for the structural objective, whereas the Rational Approximation of Material Properties (RAMP) [14] interpolation scheme is used for the conductivity objective. This work makes use of the globally convergent method of moving asymptotes (GCMMA) with three iteration loops on the solver [15]. The selection of the GCMMA solver arises from the need to resolve design-dependent loads associated with the structural objective discussed in Sec. III.C, while the relaxed number of iterations is necessary for the conductivity objective to drive solutions under the Dirichlet boundary conditions discussed in Sec. III.B.

B. Multi-Objective Formulation

This work targets increases in burn front propagation speed and the minimization of fuel geometry distortion under confinement. To provide such designs requires both maximizing thermal conduction for the improvements to the burn rate while minimizing a described structural compliance to reduce relative deflections. However, these two design properties drive designs to have significantly different features under isolated consideration. In defining quantities for each objective optimization, we then make use of Pareto optimality [16] to define a single objective with weighted components to define a family of optimized solutions. Here we write the combined objective

$$\begin{aligned}\min_{x}: f(\tilde{\boldsymbol{x}}) &= w_s f_s(\tilde{\boldsymbol{x}}) + (1-w_s) f_c(\tilde{\boldsymbol{x}}) \\ &= w_s \frac{\boldsymbol{U}(\tilde{\boldsymbol{x}})^T \boldsymbol{K}(\tilde{\boldsymbol{x}}) \boldsymbol{U}(\tilde{\boldsymbol{x}})}{f_s^*} + (1-w_s) \frac{\boldsymbol{T}(\tilde{\boldsymbol{x}})^T \boldsymbol{C}(\tilde{\boldsymbol{x}}) \boldsymbol{T}(\tilde{\boldsymbol{x}})}{f_c^*} \end{aligned} \tag{1}$$

subject to:

$$\boldsymbol{K}(\tilde{\boldsymbol{x}})\boldsymbol{U}(\tilde{\boldsymbol{x}}) = \boldsymbol{F}(\tilde{\boldsymbol{x}}) \tag{2a}$$

$$\boldsymbol{C}(\tilde{\boldsymbol{x}})\boldsymbol{T}(\tilde{\boldsymbol{x}}) = \boldsymbol{H} \tag{2b}$$

$$V_{\min}^f \leq \frac{V(\tilde{\boldsymbol{x}})}{V_0} \leq V_{\max}^f \tag{2c}$$

and

$$0 \leq \boldsymbol{x} \leq 1 \tag{2d}$$

Here $f(\tilde{\boldsymbol{x}})$ represents the combined functional for optimization over the design densities $\tilde{\boldsymbol{x}}$. Equation (1) defines f in terms of the structural and conductivity objective functions, $f_s(\tilde{\boldsymbol{x}})$ and $f_c(\tilde{\boldsymbol{x}})$, as well as a free weighting parameter, w_s, which controls the relative dominance of the individual objectives. As a result, exploring the family of

weightings defined within $0 \leq w_s \leq 1$ then supplies the full range of Pareto optimal solutions.

The structural objective f_s, frequently referred to as the structural compliance, is fully defined by the displacements $\boldsymbol{U}(\tilde{\boldsymbol{x}})$ and the stiffness $\boldsymbol{K}(\tilde{\boldsymbol{x}})$, and is constrained in Eq. (2a), where the design-dependent force vector is shown as $\boldsymbol{F}(\tilde{\boldsymbol{x}})$. The design dependency of external loads arises from the inclusion of volumetric thermal expansion, whose effect is treated as an external force. Design dependency of these thermal force terms arises from differences in the respective expansion coefficients. The thermal conductivity objective f_c, or thermal compliance, is defined by the temperatures $\boldsymbol{T}(\tilde{\boldsymbol{x}})$ and the conductivity $\boldsymbol{C}(\tilde{\boldsymbol{x}})$, and is constrained in Eq. (2b), where the heat fluxes are shown as $\boldsymbol{H}$. Both f_s^* and f_c^* are normalization factors.

The constraint in Eq. (2c) places restrictions on the volume fraction, where $V(\tilde{\boldsymbol{x}})$ is the material volume, V_0 is the total domain volume, and the lower and upper bounds of the volume fraction are defined by $V_{\min}^f$ and $V_{\max}^f$. Allowing the solver a band of allowable volume fractions better conditions solvers for the thermal expansion effects in the structural objective. Finally, the vector of design variables $\boldsymbol{x}$ describes material occupancy and must attain a value between 0 and 1.

C. Domain Filtering

Density methods are commonly combined with smoothing filters to restrict the level of detail produced during the optimization and allow designs to converge under refinement. Density filters about a given point create a weighted sum of occupancy values based on a proximity function [9,10]. For this work the un-normalized filter weights, H, are defined by a distance-based linear decay:

$$H_{ei} = \sum_{j=1}^{M} w_j \max(0, r_{\max} - r_{ej}) \tag{3}$$

where a volumetric averaging of the linear decay function is taken over the M gauss points j for every element i. The radial cutoff $r_{\min}$ is then the control parameter that restricts the allowable level of feature detailing and allows for convergence under mesh refinement. The filtered domain $\tilde{x}_e$ is then defined,

$$\tilde{x}_e = \frac{1}{\sum_{i=1}^{N} H_{ei}} \sum_{i=1}^{N} H_{ei} x_i \tag{4}$$

with the denominator ensuring that the weights are applied relative to unity.

For this work we additionally implement a generalized form of filter boundary conditions, depicted in Fig. 2 for a symmetric boundary condition. There we see the domain extent with a mesh boundary at x_B, where the domain has been shaded to indicate relative values H_{ei} about the element e. The boundary x_B' and i' are sketched as reflected pairs of x_B and i about the reflection line at x_R to highlight this as a filter with a symmetry boundary condition. This line is offset from x_B to create a null domain of width, w_N, which can be controlled to systematically create a boundary filter bias. The filters employed in traditional filter schemes introduce an uncontrollable bias that influences behavior near the domain boundaries, and further work has more recently created filters without these biases [11]. When making use of these corrected filters the structural objective explored in Sec. III.C would terminate after a single iteration with no significant reallocation of material. Using the scheme pictured in Fig. 2 allows for the controlled introduction of a boundary bias. A phenomenological discussion describing the specific effects of this null boundary as it relates to previous filters are discussed in the Appendix.

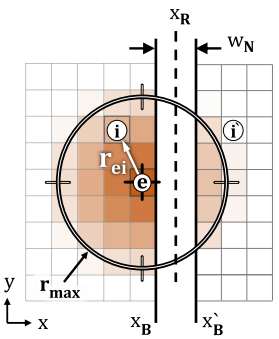

Fig. 2 Two-dimensional sketch of domain weight factor as indicated by orange shading. The insertion of a null domain of width w_N allows this scheme to generalize other filter boundary conditions.

Table 1 Fuel component material properties

HMX β Phase	Aluminum
$E = 3$ GPa [18]	$E = 69$ GPa
$\nu = 0.2153$ [18]	$\nu = 0.33$
$\alpha = 0.8 \times 10^{-5}$ K^{-1} [19]	$\alpha = 2.31 \times 10^{-5}$ K^{-1}
$K = 0.5$ W/(m · K) [20]	$K = 210$ W/(m · K)

III. Propellant RVE Setup

This work makes use of the weighted functionals of structural and thermal compliance to drive design strategies to provide a family of solid rocket fuel geometries. The required elastic and thermal material constants are described in Table 1, and the volume of aluminum is set at 19% of the total cell volume (25% by mass). This volume fraction is consistent with previous work [17] studying scale effects of aluminum particles in HMX mixtures. The selected RVE design domain is a cubic unit cell aligned to the Cartesian axis, with the z direction aligned with the normal of the progressing burn front as visualized in Fig. 3. This diagram also illustrates that the flame is outside the RVE in the positive z direction.

To fully characterize the design problem still requires a full description of geometric constraints and boundary conditions for the two objective domains. The diagrammed boundary conditions of these three domains are pictured in Fig. 4. Within each, symmetry conditions are enforced on all sides (or non–z-normal aligned) faces. This provides a consistent way of affecting a tileable system parallel to the burn front within each of the considered domains. Domain-specific boundary conditions are discussed in subsequent sections. Spatial extents of the system are 2.5 μm in all directions; however, because all material properties were characteristically linear, similar results could be achieved at different scales through a modification of the selected objective weights. It is worth noting that this argument further extends to include all transient effects of the passing combustion front, thus maintaining the validity of the designs even as the expected thermal gradients vary significantly for a given cell of solid material as the combustion front approaches.

A. Geometric Design Parameters

The primary geometry constraint, beyond the specified volume fraction, is the desired imposition on feature complexity. Here,

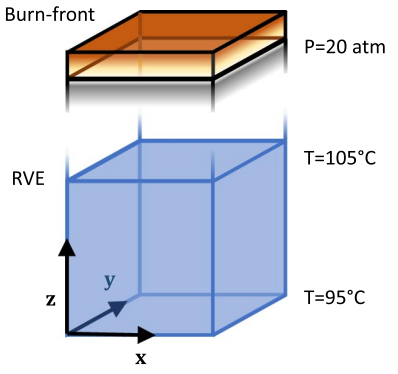

Fig. 3 Sketch of design cell with respect to the combustion zone.

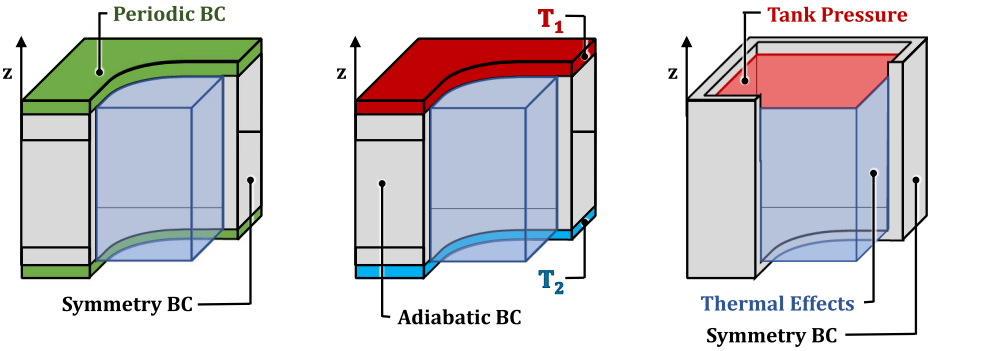

a) Geometry BC b) Thermal BC c) Structural BC and applied loads

Fig. 4 Boundary conditions and applied loads of the geometric and functional domains.

we made use of filtering radius $1/5$ of the axial domain extents to affect such restrictions. The design domain constraints pictured in Fig. 4a represent the boundary conditions as applied by the filter parameters discussed in Sec. II.C. Periodic boundary conditions along the z direction enforces consistency in creating a system of geometrically repeating cells along the burn axis. Additionally, seed points were placed at two z-aligned corners of the domain to allow for the generation of solutions to the conductivity objective. We note that placing the seed points as described is consistent with the periodic boundary condition. Finally, null boundary pads of width $w_N = r_{\min}/10$ were needed to allow for solutions to be found by the structural objective. No such padding was used on the symmetry boundary conditions.

B. Thermal Conductivity Objective

The specific aim of this work is to improve combustion rates through increases in thermal conductivity along the direction of the burn front associated with the z axis. As shown in Fig. 4b, this is enforced through fixed temperatures on each of the xy faces. The resulting gradient is defined by a 10°C difference across the domain.

C. Structural Objective

The structural objective allows for the consideration of induced stresses created by thermal expansion. Here, thermal effects are restricted to the volumetric expansion associated with a 100°C temperature rise and are uncoupled from the temperatures calculated for the thermal compliance objective. Because this expansion is affected by applying expansion loads as a function of temperature and expansion coefficients, these loads are naturally design dependent. In considering structural boundary conditions we note that within the combusting system, there is no displacement condition on the burn interface. As such, only a specified tank pressure of 20 atm is applied on the positive z face, which was not found to strongly influence the resulting designs. To fully constrain the system, the negative z face has an applied symmetry condition.

In general, the structurally dominated designs were not strongly driven, with filtered design values varying by as little as 0.1 over the whole domain. This arises because the design-dependent loads of the structural problem are ill-posed, especially in the context of high amounts of symmetry and the diffuse pressure boundary conditions. It was difficulties in this objective that drove the development and use of the defined boundary bias along the filter's periodic boundaries. For the structural objective, the boundary bias had the tendency to draw aluminum toward the biased boundaries, which is seen in subsequent results.

D. Postprocessing

Final design evaluations make use of a corrected level set of the filtered density solution to accurately reflect the design volume fraction. The projected level set is then used to calculate new occupancy values with improved delineation as compared with the filtered design variable. Linear interpolations of this new occupancy were then used to define the materials properties needed to calculate the conductivity and structural compliance for analysis. Aggregate conductivity along the burn axis was calculated using the defined change in temperature and the total thermal flux through the RVE.

IV. Results

By making use of Pareto optimality, we are subsequently presented with a family of optimal solutions. Before discussing the trends over the full Pareto front, it is helpful to first discuss a baseline of comparison, the boundary estimates of performance, and the solution outcomes of the two pure objective cases.

A. Reference Estimates and Pure Objective Solutions

Figure 5 shows the aluminum components of several fuel designs, with the negative space occupied by HMX. For the purposes of establishing a baseline estimate of particle-based geometries, Fig. 5a shows a spherical aluminum particle at the center of the domain. Figures 5b and 5c, respectively, show the optimal topology solutions for the pure structural and conductivity objectives. The seed points exist on the top and bottom of the domain at the intersection of the visualized symmetry planes that strongly affect the prominent features of both designs. In the conductivity objective these points nucleate the creation of the connecting wire seen in Fig. 5c. For the structural objective, the points act in conjunction with the introduced boundary filter bias to initiate the creation of stiffening plates with an induced internal parallel plate.

Because the primary aim of minimizing the thermal compliance objective is to increase the conductivity of the material along the burn axis, it is helpful to first calculate the upper and lower bounds of the

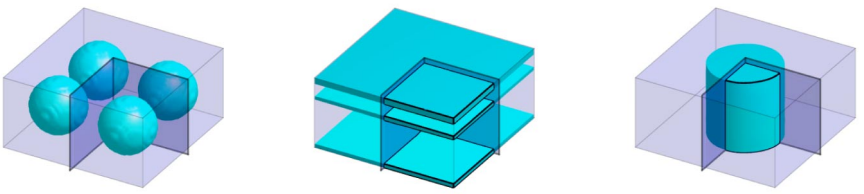

a) Reference b) Structural c) Conductivity

Fig. 5 Aluminum geometries for both the particle-based reference solution and the pure objective solutions with symmetry planes shown. HMX occupies the negative space of the visualized designs.

Table 2 Bounds and design estimates of thermal conductivities

	Thermal conductivity (W/(m · K))
Bounds	
Min	0.617
Max	40.305
Design solutions	
Reference	0.995
Structural	0.692
Conduction	40.308

possible outcomes. Using only the volume fraction V^f and the thermal conductivities listed in Table 1, such bounds are easily calculated. In general, the rule of mixtures,

$$K_{\max} = V^f_{\mathrm{HMX}} K_{\mathrm{HMX}} + V^f_{Al} K_{Al} \tag{5}$$

provides the upper bound conductivity, 40.305 W/(m · K), while the inverse rule of mixtures,

$$K_{\min} = \left(\frac{V^f_{\mathrm{HMX}}}{K_{\mathrm{HMX}}} + \frac{V^f_{Al}}{K_{Al}} \right)^{-1} \tag{6}$$

supplies the lower bound of 0.617 W/(m · K) [21]. This then provides context for the design thermal conductivities displayed in Table 2. There we see that the pure thermal objective provides a solution with a thermal conductivity nearly identical to the upper bound. We also see that both the structural objective and the reference solutions provide designs closely approximating the lower bound of conductivity. Given the need for postprocessing routines to accommodate mixed materials in the cells, these results display a remarkable correspondence in thermal conductivities between the pure objective solutions and the bounding values. The low conductivity estimate for the aluminum particle reference design affords significant possibilities for improvement.

B. Mixed Objectives

Having discussed the objectives individually, the combined objective solutions are now shown in Fig. 6, where w_s is the weight on the structural compliance function. Normally when visualizing a Pareto front, results are shown with axes resolving the respective objective terms of optimization. For this work it is both more useful, and similar in effect, to replace the thermal compliance values with the burn-axis thermal resistance. Both plotted axes are normalized to the particle reference solution for ease of comparison, with the scaled resistivity displayed in the log-scale. The front is plotted with dots

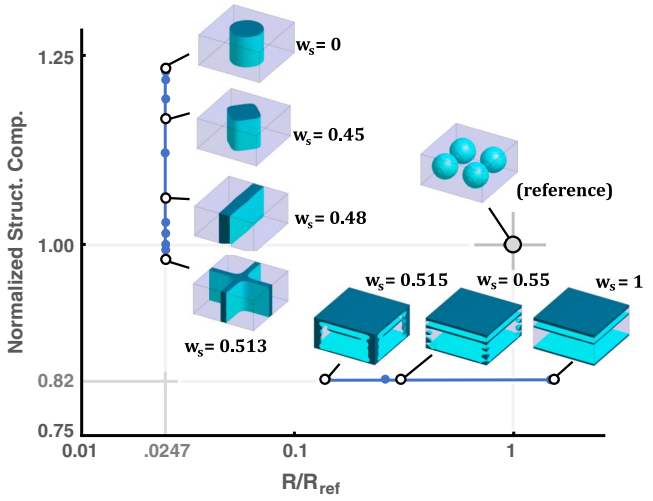

Fig. 6 Scaled resistivity and structural compliance of multi-objective weighted solutions.

Table 3 Modified parameters for HMX-Al composite fuel performance estimation

Variable/value		Description	Source
T_f	3608 K	Final gas temp.	Est. from [17]
MW	29.78 kg/kmol	Molecular weight	Est. from [17]
c_p	1.275 kJ/(kg · K)	Specific heat	Mass-weighted Al-HMX
ρ	1971 kg/m^3	Density	Vol.-weighted Al-HMX

marking found solutions, and a subset of these are selected to characterize the design family along the front.

Within the plotted front we see two families of solutions strongly segregated by whether the design is dominated by structural or conductivity objectives. Here it becomes apparent that both pure objective solutions can be directly improved in terms of their competing objective without costs in performance. For the lower branch, structural compliance varied by less than 1% while the lowest resistivity of that branch ($w_s = 0.515$) was a 91% reduction of the pure structural solution resistivity. Similarly, the upper branch saw less than 1% in deviation from the theoretical minimum resistance, while the gap in structural compliance, relative to the structurally optimal compliance value, was reduced by 71% from the design purely driven by the conductivity objective.

The character of solutions driven by the structural objective is generally plate-like in nature. To provide geometric clarity in the presence of these plates, associated designs are visualized with the seed-point locations at the outer corners of the reflected domains. Solutions dominated by the conductivity objective are made up of profiles extruded along the burn axis, which we term "wire-like." To best illustrate such designs the seed points are placed at center of the double-reflected domain. Because the primary concern of this work is the improved combustion properties of the material, this branch represents a series of burn-optimal geometries as their thermal conductivity properties have been shown to be optimal. It can be further noted that, relative to the particle reference solutions, even members of the lower solution branch are capable of offering potential improvements in combustion properties.

C. Performance Estimates

To provide context to the targeted improvements in thermal conductivity, we now seek to compare the burn propagation speeds of the wire like designs relative to the particle reference geometry. Our analysis treats the composite fuel as a monopropellant by simultaneously solving three equations for the flame thickness, mass flux rate, and the surface temperature of combustion [7]. Previously used values for HMX were used with the exception of the parameters found in Table 3 and the conductivities listed in Sec. IV.A.

Assuming a tank pressure of 20 atm yielded a flame front propagation speed of 0.76 cm/s for high-conductivity designs versus 0.50 cm/s for the reference value, an improvement of 52%. Similarly, at a tank pressure of 200 atm, high-conductivity solutions yielded a speed of 4.63 cm/s versus 3.48 cm/s for the particle reference, an improvement of 33%. These represent significant improvements in the performance of such fuels, and it suggests that the designs should receive further investigation.

V. Conclusions

This paper began by first identifying material properties of interest that might yield improvements in solid rocket propellants. Multi-objective topology optimization was then introduced to create a family of solutions that could be evaluated for improved fuel performance. Boundary conditions were defined to best reflect the structural and thermal loads present in the material before melting and combustion. To mitigate issues associated with an ill-posed structural objective constrained by design-dependent loads, a novel boundary filter bias was then introduced to provide designers control over design boundary behavior.

Design geometries bifurcated into solutions dominated by each of the objective functionals. For solutions dominated by the structural

compliance, the aluminum geometry resembled plate-like structures parallel to the combustion plane. In contrast, the thermal conductivity objective favored the creation of aluminum wires along the burn propagation axis. Both pure-objective designs were easily improved with little cost to the primary functional, but the wire-dominated designs offer the best improvements in thermal conduction. Performance estimates were used to show that wire-like designs would lead to 52 and 33% improvements in burn propagation speeds relative to a reference particle geometry for tank pressures of, respectively, 20 and 200 atm. These dramatic improvements in estimated performance demonstrate the efficacy of optimizing material properties in solid rocket propellants.

The application of topology optimization methods for the improvement of combustion and structural properties for specified chemical constituents represents a new front in the exploration for better fuel designs. With regard to the suggested designs, the scale of manufacture remains to be determined because the surface area–to–volume ratio affects combustion response. Additionally, because many of the optimal solutions were apparently influenced by the placement of symmetry boundaries, other representative volume element cell geometries should also be considered. The investigation of other fuel mixtures and chemical combinations represents a significant family of extensions to the results shown in this paper. Having provided several possible design geometries, a flame front stability analysis is needed to ensure the consistency of the resulting combustion front. As future work takes advantage of topology optimization methods in fuel design, it seems likely that new properties of interest will be incorporated into the associated solutions. In this way it seems apparent that such methods will continue to provide valuable design insights for a range of possible combustion design problems.

Appendix: Filter Boundary Bias

This appendix continues the discussion that was begun in Sec. II.C. There, a new form of controllable boundary bias was introduced as a way to offer designers a controllable bias for solutions near the boundary. To demonstrate the boundary effects on the resulting filter weights we introduce the 1D filter shown in Fig. A1a and proceed to study the insertion of a symmetry boundary at x_B. Here $\bar{H}$ represents the weights for a filter centered at x_e following normalization. For Figs. A1b, A1c, and A1d, the filtered domain is described by $x \geq x_B$, and each of these figures maintains area consistency in the filtered domain relative to the unmodified filter of Fig. A1a.

Traditionally when a filter operated over the edge of a domain extent, filters did not explicitly treat any kind of boundary condition as shown in Fig. A1b. In this and subsequent sketches, the truncated weights outside the boundary are marked by the symbol ⓑ, whereas a similarly labeled increase in form weights is affected by rescaling to unity. The result of this process is to modify the scale restriction conditions on final designs, thus inducing a filter bias that systematically favors cells with radial proximity to the domain boundaries.

Previous work [11], which found that this filter treatment of the boundaries introduced a boundary bias, showed that such effects could be attenuated by employing a domain padding consistent with a specified boundary condition. The result of this treatment, as shown in Fig. A1d, now fully accounts for the boundary at x_B being symmetric. Within this figure the domain to be reflected is marked with label?, as is the affected increases in the weights created by the reflection. As is visible in Fig. A1d there is no rescaling of weights. This alternate form of treating the boundary allows designers to condition solvers to produce solutions that are consistent, both with desired boundary criteria and with feature refinement restrictions. The ability to constrain designs to be symmetric or periodic is especially important in the context of designing an RVE.

Despite this padding strategy offering a superior design control, it was found that using such boundaries, under the diffuse and design-dependent loads discussed in Sec. III.C, resulted in solvers terminating in a single iteration, without sufficiently concentrating material. The traditional filtering methods successfully conditioned the domain for solutions, but the desired boundary condition was lost. Thus was adopted the controllable boundary scheme diagrammed in Fig. 2, whose effects on the weights are shown in Fig. A1c. Here we see the introduction of the null boundary of width w_N to create a controllable mixture of rescaling and reflection effects on the filter weights. For null boundary widths greater than the radial cutoff $r_{\min}$, the original filter of Fig. A1b is recovered; conversely Fig. A1d is the result of zeroing the width of the null domain. Ultimately the introduction of the specified null domain offers designers an ability to controllably relax design constraints in the service of allowing solvers to find solutions. While the need for such boundary treatment seems limited to specific classes of ill-posed optimization problems, the devised solution is easy to implement and conveniently encompasses both previous forms of boundary treatment.

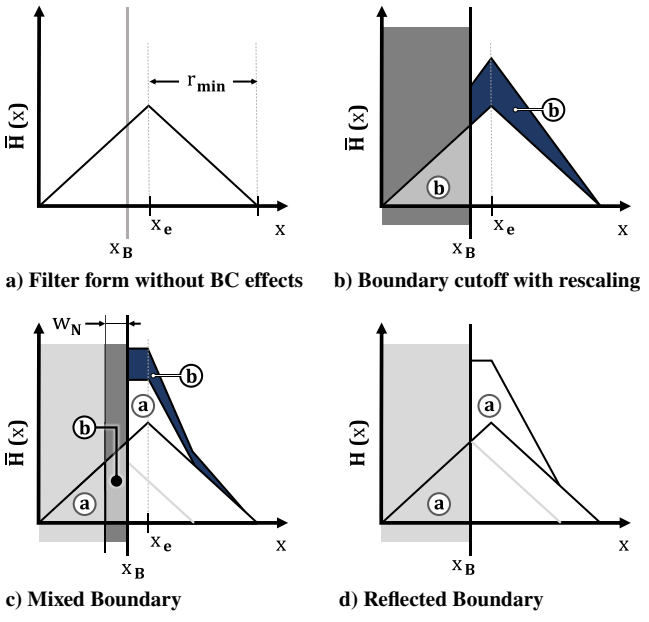

a) Filter form without BC effects b) Boundary cutoff with rescaling

c) Mixed Boundary d) Reflected Boundary

Fig. A1 1-D Filter-Form Sketches.

Acknowledgments

This work was funded by the Air Force Office of Scientific Research, by grant FA9550-17-1-02234 (program officer: Mitat Birkan). D. S. Stewart was funded by Office of Naval Research, N00014-16-1-2057.

References

[1] DeLuca, L. T., Shimada, T., Sinditskii, V. P., and Calabro, M., "Highlights of Solid Rocket Propulsion History," *Chemical Rocket Propulsion*, Springer, Cham, 2017, pp. 1015–1032.

[2] Schaedler, T. A., Jacobsen, A. J., Torrents, A., Sorensen, A. E., Lian, J., Greer, J. R., Valdevit, L., and Carter, W. B., "Ultralight Metallic Microlattices," *Science*, Vol. 334, No. 6058, 2011, pp. 962–965. doi:10.1126/science.1211649

[3] Zenou, M., Sa'ar, A., and Kotler, Z., "Digital Laser Printing of Aluminum Micro-Structure on Thermally Sensitive Substrates," *Journal of Physics D: Applied Physics*, Vol. 48, No. 20, 2015, Paper 205303. doi:10.1088/0022-3727/48/20/205303

[4] Davis, A., "Solid Propellants: The Combustion of Particles of Metal Ingredients," *Combustion and Flame*, Vol. 7, 1963, pp. 359–367. doi:10.1016/0010-2180(63)90212-8

[5] Lengelle, G., "Thermal Degradation Kinetics and Surface Pyrolysis of Vinyl Polymers," *AIAA Journal*, Vol. 8, No. 11, 1970, pp. 1989–1996. doi:10.2514/3.6036

[6] Merzhanov, A. G., and Dubovitskii, F. I., "On the Theory of Steady State Monopropellant," *Proceedings USSR Academy of Sciences*, Vol. 129, 1959, pp. 153–156.

[7] Ward, M., Son, S., and Brewster, M., "Steady Deflagration of HMX with Simple Kinetics: A Gas Phase Chain Reaction Model," *Combustion and Flame*, Vol. 114, No. 3, 1998, pp. 556–568. doi:10.1016/S0010-2180(97)00332-5

[8] Chen, T.-Y., and Wu, S.-C., "Multiobjective Optimal Topology Design of Structures," *Computational Mechanics*, Vol. 21, No. 6, 1998, pp. 483–492. doi:10.1007/s004660050327

[9] Bourdin, B., "Filters in Topology Optimization," *International Journal for Numerical Methods in Engineering*, Vol. 50, No. 9, 2001, pp. 2143–2158. doi:10.1002/(ISSN)1097-0207

[10] Bruns, T. E., and Tortorelli, D. A., "Topology Optimization of Non-Linear Elastic Structures and Compliant Mechanisms," *Computer Methods in Applied Mechanics and Engineering*, Vol. 190, Nos. 26–27, 2001, pp. 3443–3459. doi:10.1016/S0045-7825(00)00278-4

[11] Clausen, A., and Andreassen, E., "On Filter Boundary Conditions in Topology Optimization," *Structural and Multidisciplinary Optimization*, Vol. 56, No. 5, 2017, pp. 1147–1155. doi:10.1007/s00158-017-1709-1

[12] Bendsøe, M. P., "Optimal Shape Design as a Material Distribution Problem," *Structural Optimization*, Vol. 1, No. 4, 1989, pp. 193–202. doi:10.1007/BF01650949

[13] Zhou, M., and Rozvany, G., "The COC Algorithm, Part II: Topological, Geometrical and Generalized Shape Optimization," *Computer Methods in Applied Mechanics and Engineering*, Vol. 89, No. 1, 1991, pp. 309–336. doi:10.1016/0045-7825(91)90046-9

[14] Stolpe, M., and Svanberg, K., "An Alternative Interpolation Scheme for Minimum Compliance Topology Optimization," *Structural and Multidisciplinary Optimization*, Vol. 22, No. 2, 2001, pp. 116–124. doi:10.1007/s001580100129

[15] Svanberg, K., "A Class of Globally Convergent Optimization Methods Based on Conservative Convex Separable Approximations," *SIAM Journal on Optimization*, Vol. 12, No. 2, 2002, pp. 555–573. doi:10.1137/S1052623499362822

[16] Pareto, V., and Di Economia Politica, M., "Societa Editrice Libraria, Milano, Italy, 1906. Translated into English by AS Schwier as Manual of Political Economy," 1971.

[17] Muravyev, N., Frolov, Y., Pivkina, A., Monogarov, K., Ivanov, D., Meerov, D., and Fomenkov, I., "Combustion of Energetic Systems Based on HMX and Aluminum: Infuence of Particle Size and Mixing Technology," *Central European Journal of Energetic Materials*, Vol. 6, No. 2, 2009, pp. 195–210.

[18] Sewell, T. D., Bedrov, D., Menikoff, R., and Smith, G. D., "Elastic Properties of HMX," *AIP Conference Proceedings*, edited by D. F. Michael, N. T. Naresh, and H. Yasuyuki, Vol. 620, American Inst. of Physics, 2002, pp. 399–402.

[19] Saw, C. K., "Kinetics of HMX and Phase Transitions: Effects of Grain Size at Elevated Temperature," *12th International Detonation Symposium*, San Diego, CA, Aug. 2002.

[20] Dobratz, B., and Crawford, P., "LLNL Explosives Handbook - Properties of Chemical Explosives and Explosive Simulants," Lawrence Livermore National Lab. Rept. UCRL-52997, Livermore, CA, 1985.

[21] Hill, R., "Elastic Properties of Reinforced Solids: Some Theoretical Principles," *Journal of the Mechanics and Physics of Solids*, Vol. 11, No. 5, 1963, pp. 357–372. doi:10.1016/0022-5096(63)90036-X

Y. Ju
Associate Editor